High-Gain Dielectric Resonator Antenna for 6G Sub-THz Wireless Networks and Terahertz Sensing

Ashraful Haque ¹, Kamal Hossain Nahin ¹, Jun-Jiat Tiang ^{2,*}, Mehidy Hasan ³, Narinderjit Singh Sawaran Singh ⁴, and Abdul Kader Jilani ⁵

¹ Department of Electrical and Electronic Engineering, Daffodil International University, Dhaka, 1207 Bangladesh
² Centre for Wireless Technology, CoE for Intelligent Network, Faculty of Artificial Intelligence and Engineering, Multimedia University, Persiaran Multimedia, 63100 Cyberjaya, Selangor, Malaysia

³ Department of Engineering Management, Trine University, Angola, IN, USA

⁴ Faculty of Data Science and Information Technology, INTI International University, Persiaran Perdana BBN, Putra Nilai, Negeri Sembilan, Malaysia

⁵ Faculty of Physics and Astronomy, Friedrich Schiller University Jena, Germany Email: limon.ashraf@gmail.com (A.H.); kamal33-1242@diu.edu.bd (K.H.N.); jjtiang@mmu.edu.my (J-J.T.); mhasan222@my.trine.edu (M.H.); narinderjits.sawaran@newinti.edu.my (N.S.S.S.); md.abdul.jilani@uni-jena.de (A.K.J.)

*Corresponding author

Abstract—This article presents the design and evaluation of a Rectangular Dielectric Resonator Antenna (RDRA) for sub-THz applications, specifically at a frequency of 0.49 THz. The antenna exhibits promising performance with a return loss of -35.45 dB, a bandwidth of 351 GHz, and an efficiency of approximately 85%. With a compact size of 59 µm × 59 µm, the RDRA offers a high-performance solution for nextgeneration wireless communication systems. The antenna's performance was assessed through software simulations, an RLC equivalent circuit model, and Machine Learning (ML) techniques. The resonance frequencies predicted by the Resistor, Inductor, Capacitor (RLC) model, simulated using Advanced Design System (ADS) Agilent software, align closely with those from other modeling tools, validating the accuracy of the design. Furthermore, five regression-based ML models were developed to predict the dielectric antenna's gain, with the XGB regression model demonstrating the best prediction accuracy. The study also explores the efficacy of the ML models using several evaluation metrics, including variance score, R-squared, Mean Square Error (MSE), and Root Mean Square Error (RMSE). The results highlight the potential of the RDRA for sub-THz applications, such as ultra-fast wireless communication and high-resolution imaging, with ML enhancing the design optimization process.

Keywords—6G, Advanced Design System (ADS), Dielectric Resonator Antenna, Machine Learning, Resistor, Inductor, Capacitor (RLC)

Manuscript received March 17, 2025; revised April 25, 2025; accepted May 13, 2025; published October 21, 2025.

I. INTRODUCTION

The Sixth Generation (6G) of wireless communication is set to revolutionize global connectivity by overcoming the limitations of its predecessors and enabling ultra-fast data rates, seamless global coverage, and low-latency services [1]. Wireless technology has evolved from the analog voice transmission of the First Generation (1G) to the high-speed broadband connectivity of 5G. While 5G introduced significant improvements, including enhanced mobile broadband (eMBB) and Ultra-Reliable Low-Latency Communication (URLLC), it still faces major challenges such as spectrum congestion, energy inefficiency, and limited support for data rates beyond gigabits per second [2]. To address these limitations, 6G is expected to utilize the sub-terahertz (sub-THz) frequency range (0.1-1 THz), which offers wider bandwidths, improved spectral efficiency, and the potential for Terabit-Per-Second (Tbps) data transmission [3]. These advancements will support next-generation applications such as wireless backhaul, high-resolution sensing, holographic communication, space-air-ground integrated networks, and intelligent transportation systems [4]. However, operating at sub-THz and THz frequencies introduces new challenges, including high path loss, atmospheric absorption, and hardware limitations, requiring innovative solutions in antenna design, signal processing, and beamforming techniques [5]. Additionally, the development of highly efficient power amplifiers, lowloss transmission lines, and advanced modulation techniques are crucial for unlocking the full potential of THz communication.

To enable efficient 6G communication, extensive research is being conducted on sub-THz and THz antennas [6]. Traditional metallic antennas face increasing losses at higher frequencies, making alternative solutions such as metasurfaces, leaky-wave antennas, and Dielectric Resonator Antennas (DRAs) more viable. DRAs, for instance, offer high efficiency and minimal conduction loss, making them promising candidates for THz applications [7]. However, other technologies such as plasmonic antennas, Reconfigurable Intelligent Surfaces (RIS), and graphene-based antennas are also being explored due to their potential for enhanced directivity, tunability, and miniaturization. Additionally, phased-array antennas and beamforming techniques are being developed to mitigate high propagation losses and extend communication range in THz frequencies. Furthermore, advancements in Machine Learning (ML) and Artificial Intelligence (AI) are transforming antenna design, allowing for optimization of gain, bandwidth, and efficiency while reducing design complexity [8]. The integration of ML-driven models with electromagnetic simulations is accelerating the development of highperformance THz antennas [9]. The combination of advanced antenna design, AI-driven optimizations, and next-generation fabrication techniques will be critical in overcoming the current challenges of THz communication. As research continues, the successful implementation of these technologies will define the future of 6G networks, enabling ultra-fast, reliable, and energy-efficient wireless communication for diverse applications [10].

In this research paper, a Rectangular Dielectric Resonator Antenna (RDRA) has been proposed with a resonant frequency of 0.49 THz and a return loss of -35.45 dB. The antenna exhibits a wide bandwidth of 351 GHz, measured at -10 dB, ensuring high data transmission capacity. Additionally, the RDRA achieves an efficiency of 85% with a gain of 9 dB and a directivity of 10.41 dB, making it a strong candidate for next-generation 6G wireless communication. The combination of high efficiency, significant gain, and wide bandwidth enhances signal strength, coverage, and reliability, making the proposed RDRA suitable for applications such as ultra-fast wireless backhaul, high-resolution imaging, and secure

short-range communications in the Terahertz (THz) frequency range.

The performance of the antenna is designed and finetuned using CST MWS simulation software. The R-L-C equivalent circuit is used to verify the return loss level in the Advance Design System (ADS) circuit simulation tool. An innovative method for forecasting directivity and gain using multiple regression techniques has recently been investigated using the CST Electromagnetic (EM) modeling tool.

Table I provides a comparative analysis of the proposed antenna with previously reported designs [11-15]. The proposed antenna achieves a superior return loss of -35.45 dB, which is better than -20 dB, -29 dB, -50 dB, and -30 dB reported in in the literature [11–13, 15]. The proposed antenna achieves the highest bandwidth of 0.351 THz, which is significantly higher than 0.1 THz, 0.017 THz, 0.15 THz, 0.114 THz, and 0.11 THz, as reported in the cited articles [11-15]. In terms of gain, the proposed antenna reaches 9 dB, outperforming the 6.3 dB, 4.1 dB, 7.15 dB, 4.4 dB, and 4.45 dB from the other works. Additionally, the proposed antenna achieves an efficiency of 83.17%, which is higher than 34%, 38%, and 75% from references [11-13], respectively. Unlike the previously reported designs, the proposed antenna stands out by incorporating advanced techniques such as Machine Learning (ML) and an RLC circuit model, which are completely absent in the other works. These unique features not only enhance the overall performance of the proposed antenna but also make it highly efficient and adaptable for future THz communication systems, which was not explored in the prior designs.

The proposed DRA antenna at the THz frequency shows superior performance compared to the microstrip patch antenna, as shown in Table I. The improved performance could be due to low metallic loss as the dielectric material is used instead of metal patches. However, DRA offers higher bandwidth by nature for its structure. Additionally, we introduced a novel feedline design to excite the DRA, which significantly improves impedance matching and contributes to the overall enhanced performance of the antenna.

Defended
TABLE I. PERFORMANCE COMPARISONS WITH THE RECENT STATE OF THE ART

_	References					
Parameter	[11]	[12]	[13]	[14]	[15]	Proposed
Return Loss (dB)	-20	-29	-50	-	-30	-35.45
Operating Frequency (THz)	0.19-0.2	0.303-0.32	0.7-0.85	0.093-0.207	1.76 -1.87	0.31- 0.661
Bandwidth (THz)	0.1	0.017	0.15	0.114	0.11	0.351
Gain (dB)	6.3	4.1	7.15	4.4	4.45	9
Efficiency (%)	34	38	75	98	_	83.17
Size (W×L) μm ²	2000 × 1350	550 × 1100	600 × 700	1000 × 1000	60 × 40	59 × 59
ML	No	No	No	No	No	Yes
RLC	no	No	No	No	No	Yes
Substrate Material	Polyimide	SiO2	Rogers RT 6006	Rogers RO4835	SiO2	Polyi Mide

II. DESIGN METHODOLOGY

Fig. 1 shows the microstrip transmission line that supplies power to the antenna's installed DRA. A 4 µm thick and 3.5 dielectric constant polyimide substrate, measuring 59 µm in height and 59 µm in length, supports the microstrip line. The Resonator antenna is 11 µm in height and uses ground and patch copper with a 0.035 μm thickness each. This proposed DRA geometry can be used as a basis for the design and fabrication of a practical antenna for use in various applications. By modifying the dimensions of the DRA and the substrate, it may be possible to achieve specific performance characteristics, such as a desired operating frequency, radiation pattern, or impedance matching. These modifications can be optimized using simulation tools and experimental measurements to validate the antenna's performance.

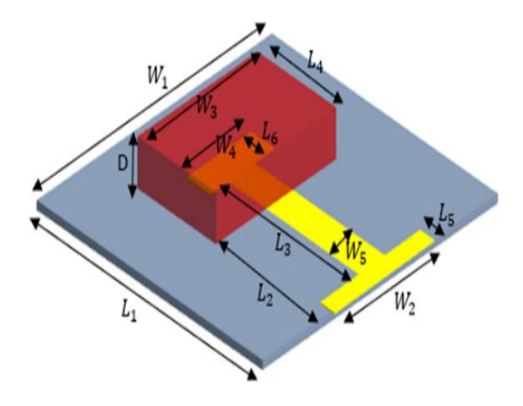


Fig. 1. Three-dimensional view of proposed DRA.

The resonance frequency of the fundamental mode is calculated by the given [16].

$$f_0 = \frac{c}{2\pi\sqrt{a}} \sqrt{k_x^2 + k_y^2 + k_z^2} \tag{1}$$

$$f_{0} = \frac{c}{2\pi\sqrt{\varepsilon_{r}}} \sqrt{k_{x}^{2} + k_{y}^{2} + k_{z}^{2}}$$
(1)

$$k_{x} tan \frac{k_{x}d}{2} = \sqrt{((\varepsilon_{r} - 1)k_{0}^{2} - k_{x}^{2})}$$
(2)

$$k_{0} = \frac{2\pi}{\lambda_{0}}, k_{y} = \frac{\pi}{w}, k_{z} = \frac{\pi}{b}$$
(3)

$$k_0 = \frac{2\pi}{\lambda}$$
, $k_y = \frac{\pi}{W}$, $k_z = \frac{\pi}{h}$ (3)

where, k_0 is the free space wavenumber and k_x , k_y , and k_z are the wavenumber along x, y, and z coordinates, ε_r is the dielectric constant of DR, w is the width of DR, h = b/2is the height of DR, b = length of the DR, and λ_0 is freespace wavelength.

The dimension of feed is determined by tuning it to achieve the desired characteristic impedance (Zc) using Eq. (6) [17].

$$Zc \begin{cases} \frac{60}{\sqrt{\epsilon_{reff}}} \ln\left[\frac{8h}{f\omega} + \frac{fw}{4h}\right] & ; \frac{fw}{h} \leq h \\ \frac{120\pi}{\sqrt{\epsilon_{reff}} \left[\frac{fw}{h} + 1.393 + 0.667 \ln\left(\frac{fw}{h} + 1.444\right)\right]} & ; \frac{fw}{h} > 1 \end{cases}$$

$$(4)$$

The length of the feed line is calculated using Eq. (7).

$$L_0 = \frac{1}{4}\lambda_g \tag{5}$$

where,
$$\lambda_g = \frac{c}{f_r \sqrt{\epsilon_r}}$$

The dimensions of the ground plane are determined by the Equations below:

$$Lg = 6h + L \tag{6}$$

$$Wg = 6h + W \tag{7}$$

In the given context, the symbols used represent the following quantities: λ represents the wavelength, c represents the speed of light, 'f' denotes frequency, ε_r and h denotes dielectric constant, the Effective Dielectric Constant is represented by ε_{eff}

These values represent the ideal setting of the antenna, all measurements are in micrometers (μm): L1 = 59, L2 = 17.5, L3 = 37, L4 = 20, L5 = 2, W1 = 59, W2 = 20, W3 = 2028, W4 = 10, W5 = 4.

When the feedline is energized, the square-shaped dielectric resonator traps and confines waves, creating standing wave patterns at a specific frequency (0.49 THz). These waves generate fringing fields at the resonator's edges, which couple with free space and radiate efficiently. The polyimide substrate supports the structure and reduces signal loss, while the ground plane reflects the waves back into the resonator and helps direct the radiation upward.

III. RESULT ANALYSIS OF THE PROPOSED DRA

High Return Loss means that the antenna can broadcast and receive more RF energy. Optimum performance needs a return loss of less than 10 decibels (dB) demonstrates that the proposed antenna can resonate at 0.493 THz, with corresponding Return Loss values of -35.45dB. The calculated bandwidth at -10 dB is 351 GHz. These results indicate that the proposed antenna is capable of high performance, with good Return Loss values and a sufficiently wide bandwidth to support various 6G communication applications. The design and simulation of the proposed antenna were conducted using CST Studio Suite software. To verify the simulation results, the same parameters were used to design the antenna in HFSS and FEKO software. The comparison of the S11, obtained from the three software is presented in Fig. 2. Gain and Directivity are crucial antenna performance variables. Gain measures power transferred to the primary beam, while directivity measures radiation concentration in a certain direction [18]. Fig. 3 displays the computed gain and directivity at the resonant frequency, which are 9dB and 10.41 dBi, respectively. An antenna's radiation efficiency is calculated by dividing its power output by its excitation port power [19].

The planned DRA's Agilent ADS RLC model is displayed here. Therefore, R, L, and C are chosen to match the transmission line's 50 ohms characteristic impedance with the antenna's equivalent impedance [20]. The proposed antennas patch equivalent circuit is presented. in Fig. 4 by a parallel RLC circuit of resistance R1, inductance L1, capacitance C1, and another parallel circuit of resistance R2, inductance L2, and capacitance C2 connected in series. The resonator electric circuit equivalent is shown in Fig. 5. In parallel with the resonator

circuit, C3, L3, C5, and L5 in series. Finally, the equivalent circuit of the proposed DRA is created in Fig. 6, using the resonator and patch circuit. While using the S-parameter lump, the frequency range is cleared from 0 THz to 1 THz in 0.2 THz increases. The resonant circuit has a 0.45 THz resonance frequency and a return loss of -47 dB. Comparative evaluation is used to verify Agilent ADS simulation accuracy. This is done by comparing parallel circuit and CST simulation results, focusing on the S11 parameter. In Fig. 7, the resonance frequencies of the CST and ADS are identical, and the R-L-C parameter is provided in Table II.

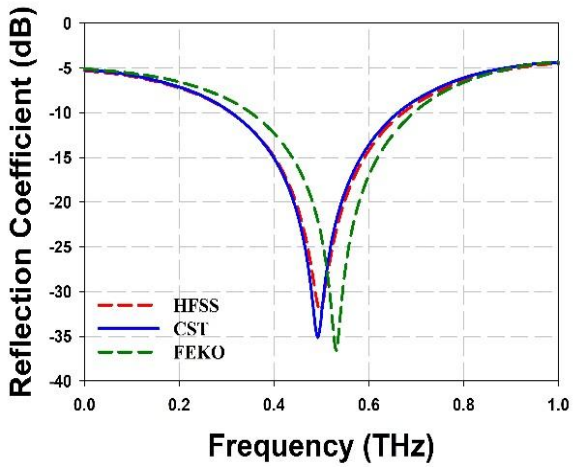


Fig. 2. Comparing reflection coefficient using CST, HFSS and Altair Feko of the proposed DRA.

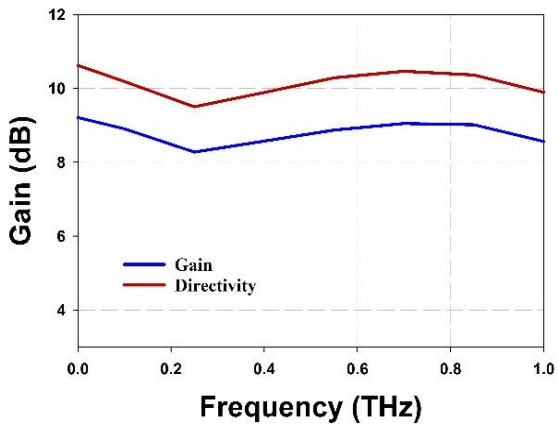


Fig. 3. Comparing gain and directivity of the proposed DRA.

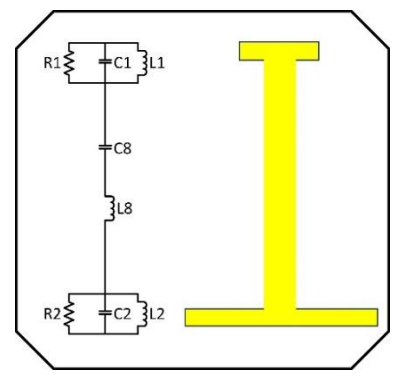


Fig. 4. Equivalent circuit of the patch.

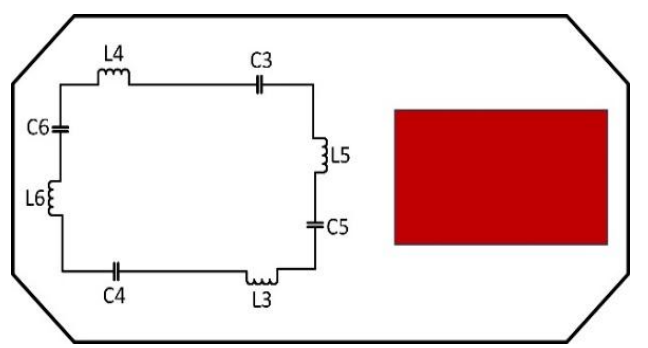


Fig. 5. Equivalent circuit of the resonator.

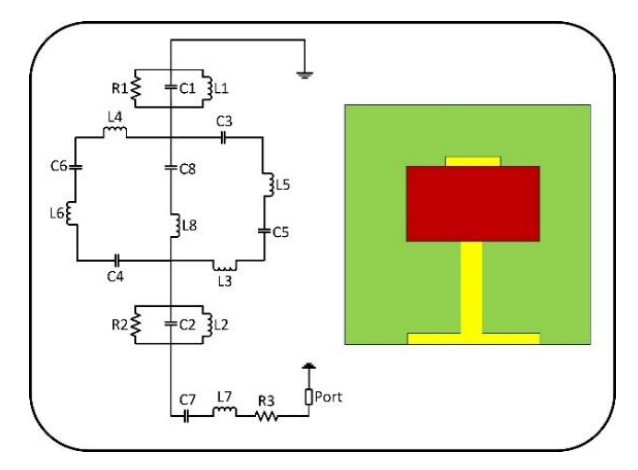


Fig. 6. Final equivalent circuit of the proposed DRA

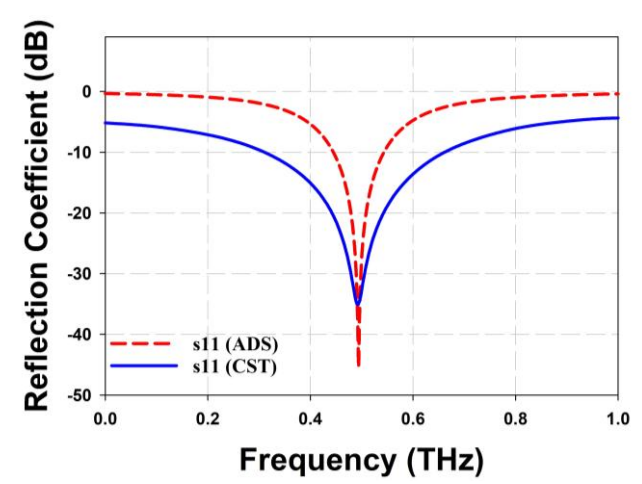


Fig. 7. Comparing simulated results using CST and ADS equivalent circuit.

TABLE II. VALUE OF THE RLC PARAMETER

Parameter	Value	Parameter	Value	Parameter	Value
L1	0.2 pH	С3	3 pF	C7	0.1 pF
C1	100 pF	L4	1.1 pH	L7	9.9 pH
R1	51 ohms	C4	003 pF	C8	11 pF
L2	23 pH	L5	3 pH	L8	0.1 pH
C2	31 pF	C5	30 pF	R3	50 ohms
R2	50 ohms	С6	3.2 pF		
L3	1 pH	L6	13.5 pH		

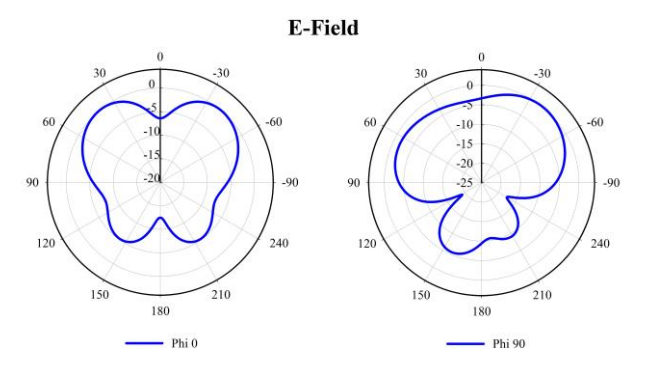


Fig. 8. 2D radiation pattern at 0.45 THz (E-field).

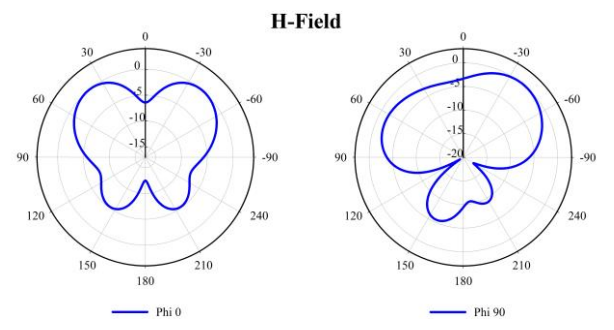


Fig. 9. 2D radiation pattern at 0.45 THz (H-field).

This is a representation of the fields (both electric and magnetic) at an angle of 0 degrees and 90 degrees [21]. Fig. 8 shows the E-field and Fig. 9 shows the H-field of the proposed DRA. The primary focuses main lobe of E-field and H-field patterns are located at coordinates (41°, 39°) and $(41^{\circ}, 39^{\circ})$, respectively, at an angle of = $(0^{\circ}, 90^{\circ})$. At an angle of 90 degrees and 0 degrees, the magnitudes are 18.9 dB V/m and 15.8 dB V/m, respectively, and -32.7 dBA/m and -35.7 dBA/m, respectively. According to the layout of radiation patterns, the suggested antenna emits radiation in all directions. The half power beamwidth or 3 dB angle beam width for 0 degrees is 57.9, and the side part near is -5.2 dB. In contrast, the 3 dB angular beam width for 90 degrees is 71.6, and the side lobe level is -1.8dB. As a result, based on the study that was presented, it is the DRA that is appropriate for 6G applications.

IV. MACHINE LEARNING

ML algorithms are skilled at handling data with several dimensions and types. Due to these unique qualities, ML is being used to solve classification and optimization issues in the Electromagnetic (EM) domain, most notably for antennas. That's why a sizable chunk of the present study is devoted to machine learning methods. Many modern electromagnetics researchers are keen on exploring the use of various machine learning methods in antenna system design and optimization. The optimisation process is sped up by using deterioration methods, as their ML assessment is much earlier than the mathematical solution.

The approach is split into two halves. First, the N79-band antenna is designed in CST, a simulation, and the parametric sweep dataset is extracted as shown in Fig. 10. We simulate the proposed antenna's gain and directivity

using CST MWS and use multiple regression ML methods to 100 data samples. Approximately 80% are utilized during the training phase, while 20% are reserved for the testing phase. For the training and testing sets, the sample sizes are 80 and 20, respectively. The length, width, and height dimensions of the substrate, as well as the thickness of the patch, are all input variables in the dataset we utilized; the gain and directivity parameter are the primary output as shown in Fig. 11. Finally, a method for machine learning is applied to the training dataset, and this algorithm considers both the features and the labels. After the training and validation of the model has been finished, it will be possible to utilize the model to make accurate predictions of inputs such as realized gain.

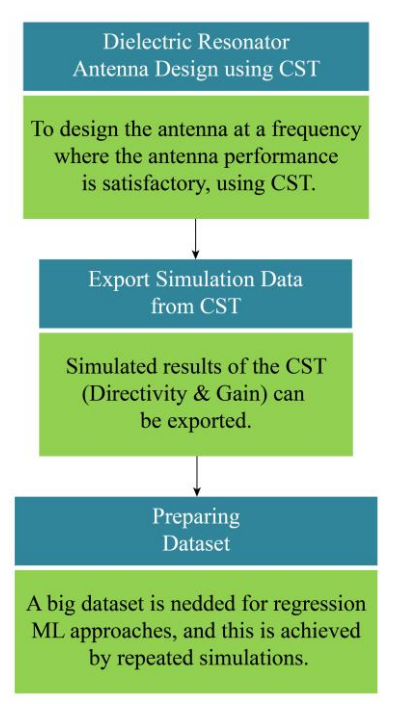


Fig. 10. Data acquisition workflow for machine learning.

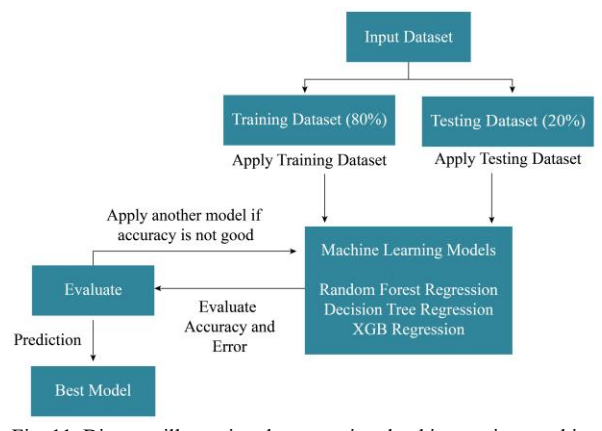


Fig. 11. Diagram illustrating the stages involved in creating machine learning.

Linear Regression: The purpose of linear regression [22] is to model the relationship among two variables by attempting to fit a linear equation to data that can be observed. The first variable is an expressive flexible, and

the second variable is the dependent variable in the model.

Decision Tree Regression: A decision tree is a model honed to fit within the framework of a tree. After then, one uses this model to make projections about the data that will take place in the future and to consistently generate relevant results [23].

Gaussian Process Regression: The method of supervised machine learning known as Gaussian process regression, more commonly abbreviated as GPR, can be utilized for a variety of tasks, including regression and classification, among others [24].

Random Forest Regression: The process of employing random forests for classification and regression requires the generation of a set of tree forecasts, which is referred to as random forest regression. Each tree forecaster is built with an unidentified vector that is chosen independently of the input vector throughout the construction process [25].

XGB Regression: The process of training on big datasets is sped up by the constructed in optimizations that are included in XGBoost. Its cutting-edge capabilities include the capacity to deal with missing values, regularization, and parallel processing, to name a few. With the assistance of XGBoost [26], antenna designers can generate predictions regarding antenna attributes like radiation patterns, gain, and directivity based on data that was either simulated or tested.

Performance Measurement Metrics: In regression, error is the most popular measure of performance. The performance of each algorithm was compared using a wide variety of statistical measures. The performance of the algorithms was evaluated using several statistical metrics, with the results being compared to one another. We measured how well our models predicted outcomes using a battery of five different statistics: (RMSE), (R²), variance score, and (MAE) were utilized to determine how accurate the forecasts were [27].

In a regression issue, the Mean Absolute Error (MAE) is a metric that is used to quantify the difference among the predicted values and the actual values. A smaller Mean Absolute Error (MAE) is indicative of high accuracy in forecasting the dependent variable. A representation of the MAE [28] formulation can be seen in Eq. (8).

$$AE = \frac{1}{n} \sum_{i=1}^{n} |Pi - Oi| \tag{8}$$

where, n = number of errors, |Pi-Oi| = error absolute

The mean squared error (also known as MSE) is the most typical representation of the regression loss function. The amount of the loss is strongminded by taking the usual across all the data opinions of the squared changes that exist among the actual values and the expected values. The MSE [29] formulation is shown in Eq. (9), as indicated.

$$MSE = \frac{1}{N} \sum_{i=1}^{N} (\hat{y}_i - y_i)^2$$
 (9)

Root Mean Squared Error is the abbreviation for RMSE. When appraising the efficacy of a predictive model, particularly in the context of regression tasks, it is a statistic that is frequently put to use. The Root-MeanSquare Error (RMSE) is measured by comparing the values that were expected by the model to the values that were found in the data [30].

$$RMSE = \sqrt{\frac{1}{n} \sum_{i=1}^{n} (Pi - Oi)^2}$$
 (10)

The coefficient of resolution (R^2) is another popular metric used in regression analysis to assess the quality of a model's fit to the data. The segment of the reliant on variable's modification that can be qualified to the model's independent variables is calculated. The range of R^2 is from 0 to 1, and it is defined as follows: If the coefficient of determination, or R^2 , is zero, it means that the typical does not describe any of the alterations in the reliant on adjustable and that utilizing the model's predictions is the same as using the mean of the dependent variable [31].

$$R^{2} = 1 - \frac{\sum_{i=1}^{N} (y_{i} - \hat{y}_{i})^{2}}{\sum_{i=1}^{N} (y_{i} - \hat{y}_{i})^{2}}$$
(11)

A regression model's efficacy can be measured using the Help of Explained Variance Score. The fraction of the reliant on variable's variation that can be described for by the model is calculated. The variance of the dependent variable is used in calculating the Explained Variance Score, as opposed to the overall variance as in the case of R-squared [32]. To determine your Explained Variance Score, use this formula.

explained variance
$$(y, \hat{y}) = 1 - \frac{Var(y-\hat{y})}{Var(y)}$$
 (12)

V. RESULT ANALYSIS M/L

Table III compares the five deterioration models' gain prediction accuracy. Furthermore, this comparison was made using five separate criteria. In XGB Regression, the values for MAE, MSE, and RMSE are 5.43873%,. 0.52921%, and 7.09791%, respectively. The best performance is seen in XGB Regression, with an R² of 93.4867% and a variance of 93.7669%. Figs. 12 and 13 features a bar chart comparing the models' performance. The expected result is like the simulated result, as shown in Fig. 14 XGB was chosen to predict gain better than other ML models. Their predicted and the actual gain of XGB are only slightly different, as has been shown.

TABLE III. THE GAIN PREDICTION PERFORMANCE

Algorithms	MAE (%)	MSE (%)	RMSE (%)	R SQUARE(%)	VAR SCORE (%)
Linear Regression	8.241	1.786	13.364	76.911	78.657
Decision Tree	14.568	16.151	40.188	65.61	67. 67
Regression Random Forest Regression	8.113	1.057	0.283	86.33	87.533
Gaussian Process Regression	8.044	16.954	13.021	78.08	79. 75
XGB Regression	5.439	0.504	7.098	93.487	93.767

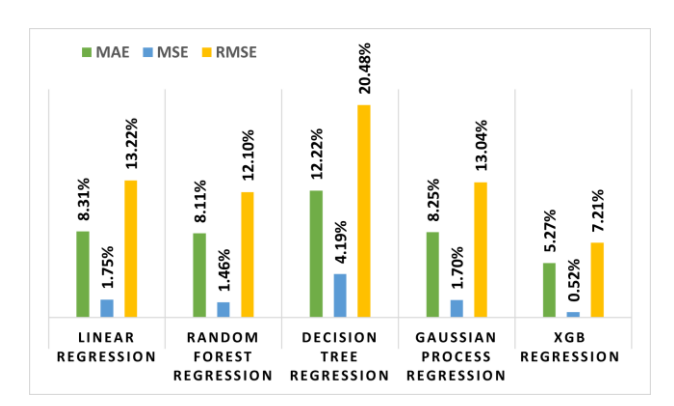


Fig. 12. Error metrics bar chart of ML regression (Gain).

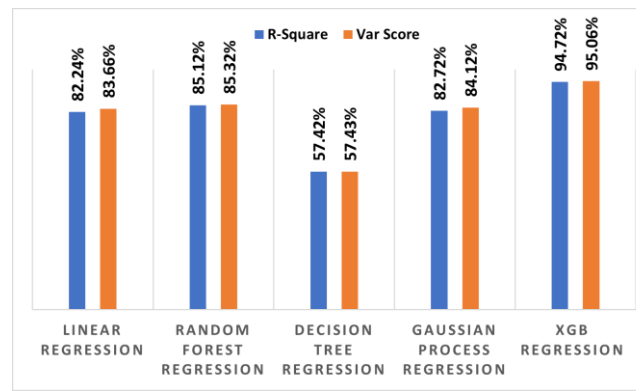


Fig. 13. Accuracy comparative bar chart of ML regression (Gain).

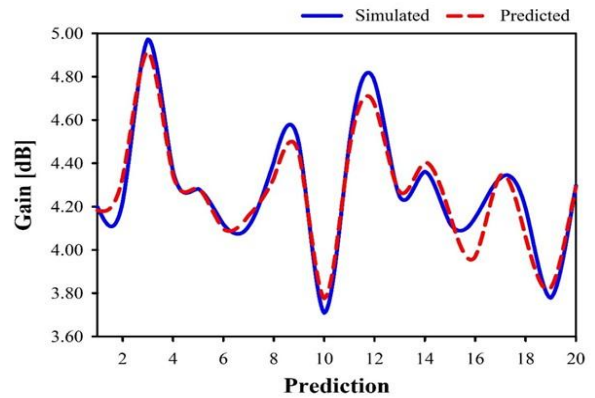


Fig. 14. Simulated vs predicted gain using XGB regression.

VI. CONCLUSION

This Research Integrates Simulation, RLC equivalent circuit modeling, and Machine Learning (ML) techniques to evaluate the performance of the proposed Rectangular Dielectric Resonator Antenna (RDRA) for sub-THz applications. The antenna was initially designed and analyzed using CST software, with an RLC equivalent model developed in ADS Agilent to validate its resonance characteristics. The close agreement between the simulation results and the equivalent circuit model confirms the accuracy of the proposed design methodology. Additionally, five ML models were developed to predict the gain and directivity of the dielectric antenna, with the XGB regression model demonstrating superior predictive accuracy. The strong correlation between simulation and ML predictions highlights the reliability of the proposed

approach in optimizing antenna performance. The designed RDRA exhibits high efficiency, substantial bandwidth, and enhanced gain, making it a promising candidate for next-generation 6G wireless communication. With its suitability for sub-THz and THz frequency applications, including ultra-fast wireless networks, highresolution imaging, and space-air-ground integrated systems, this antenna model offers a robust solution to address the challenges of future wireless technologies. The integration of ML-driven optimization techniques further enhances the design and evaluation process, paving the way for more adaptive and intelligent antenna solutions. The proposed antenna structure has good potential for mass manufacture from a production perspective. Alumina ceramic, copper, and polyimide are examples of inexpensive materials that guarantee material affordability. Additionally, the antenna design works with common microfabrication methods that are currently widely used in semiconductor **MEMS** and photolithography and wet/dry etching. These features enable the design's cost-effectiveness and scalability, which qualify it for commercial use in terahertz communication systems.

CONFLICT OF INTEREST

The authors declare no conflict of interest.

AUTHOR CONTRIBUTIONS

Ashraful Haque: Conceptualization, Methodology, Formal analysis, Software; Kamal Hossain Nahin: Conceptualization, Methodology, Writing – Original Draft, Writing – Review and Editing; Jun-Jiat Tiang: Formal analysis, Project administration, Validation; Mehidy Hasan: Supervision, Validation, Writing – Review Narinderjit Singh Sawaran Singh: Resources, Supervision; Abdul Kader Jilani: Methodology, Formal analysis, Software; and Editing; all authors had approved the final version.

ACKNOWLEDGMENT

The authors extend their appreciation to acknowledge the Information and Communication Technology Division (ICTD), Agargaon, Dhaka, Bangladesh, for funding this research work through grant number No: 56.00.0000.000.052.33.0003.24-130.

REFERENCES

- [1] M. A. Haque *et al.*, "Multiband THz MIMO antenna with regression machine learning techniques for isolation prediction in IoT applications," *Sci. Rep.*, vol. 15, no. 1, 7701, Mar. 2025. doi: 10.1038/s41598-025-89962-6
- [2] K. H. Nahin et al., "Performance prediction and optimization of a high-efficiency tessellated diamond fractal MIMO antenna for terahertz 6G communication using machine learning approaches," Sci. Rep., vol. 15, no. 1, 4215, Feb. 2025. doi: 10.1038/s41598-025-88174-2

- [3] J. H. Nirob et al., "Dual-band MIMO antenna for wideband THz communication in future 6G applications," TELKOMNIKA, vol. 23, no. 2, p. 295, Apr. 2025. doi: 10.12928/telkomnika.v23i2.26553
- [4] K. Ahmed et al., "Graphene-based THz antenna with a wide bandwidth for future 6G short-range communication," *Telkomnika*, vol. 23, no. 2, p. 306, Apr. 2025. doi: 10.12928/telkomnika.v23i2.26562
- [5] M. A. Haque et al., "Regression supervised model techniques THz MIMO antenna for 6G wireless communication and IoT application with isolation prediction," *Results in Engineering*, 103507, Nov. 2024. doi: 10.1016/j.rineng.2024.103507
- [6] J. H. Nirob et al., "Optimized tri-band MIMO antenna design for 6G terahertz applications and future connectivity," *Telkomnika*, vol. 23, no. 2, p. 553, Apr. 2025. doi: 10.12928/telkomnika.v23i2.26579
- [7] N. R. S. Yaduvanshi, A. K. Kushwaha, and A. K. Pandit, "Terahertz rectangular DRA for high-speed communication applications," *Journal of Discrete Mathematical Sciences and Cryptography*, vol. 24, no. 5, pp. 1205–1214, Jul. 2021.
- [8] M. A. Haque et al., "Machine learning-based novel-shaped THz MIMO antenna with a slotted ground plane for future 6G applications," Sci. Rep., vol. 14, no. 1, 32162, Dec. 2024. doi: 10.1038/s41598-024-79332-z
- [9] Y. Jiang et al., "Machine learning and application in terahertz technology: A review on achievements and future challenges," *IEEE Access*, vol. 10, pp. 53761–53776, 2022. doi: 10.1109/ACCESS.2022.3174595
- [10] M. A. Haque et al., "Performance improvement of THz MIMO antenna with graphene and prediction bandwidth through machine learning analysis for 6G application.," Results in Engineering, 103216, Oct. 2024. doi: 10.1016/j.rineng.2024.103216
- [11] M. Alibakhshikenari *et al.*, "High-isolation antenna array using SIW and realized with a graphene layer for sub-terahertz wireless applications," *Sci. Rep.*, vol. 11, no. 1, 10218, 2021.
- [12] H. Zhu, X. Li, Z. Qi, and J. Xiao, "A 320 GHz octagonal shorted annular ring on-chip antenna array," *IEEE Access*, vol. 8, pp. 84282–84289, 2020. doi: 10.1109/ACCESS.2020.2991868.
- [13] R. H. Mahmud, "Terahertz microstrip patch antennas for the surveillance applications," *KJAR*, vol. 5, no. 1, pp. 16–27, Apr. 2020. doi: 10.24017/science.2020.1.2
- [14] T. Okan, "High efficiency unslotted ultra-wideband microstrip antenna for sub-terahertz short range wireless communication systems," *Optik*, vol. 242, 166859, Sep. 2021.
- [15] G. Varshney, S. Gotra, V. S. Pandey, and R. S. Yaduvanshi, "Proximity-coupled two-port multi-input-multi-output graphene antenna with pattern diversity for THz applications," *Nano Communication Networks*, vol. 21, 100246, Sep. 2019. doi: 10.1016/j.nancom.2019.05.003
- [16] P. R. Meher, B. R. Behera, and S. K. Mishra, "Design and its state-of-the-art of different shaped dielectric resonator antennas at millimeter-wave frequency band," *Int. J. RF Microw Comput Aided Eng.*, vol. 30, no. 7, Jul. 2020.
- [17] A. H. Rambe, M. L. Asri, S. Suherman, and R. Harahap, "Design and simulation of rectangular patch microstrip antenna with inset feed for S-band application," *IOP Conf. Ser.: Mater. Sci. Eng.*, vol. 725, no. 1, 012056, Jan. 2020.
- [18] M. A. Haque et al., "Machine learning-based technique for gain prediction of mm-wave miniaturized 5G MIMO slotted antenna

- array with high isolation characteristics," *Sci. Rep.*, vol. 15, no. 1, p. 276. Jan. 2025.
- [19] M. A. Haque et al., "Machine learning-based technique for directivity prediction of a compact and highly efficient 4-port MIMO antenna for 5G millimeter wave applications," Results in Engineering, 103106, Oct. 2024.
- [20] M. A. Haque et al., "Machine learning based compact MIMO antenna array for 38 GHz millimeter wave application with robust isolation and high efficiency performance," Results in Engineering, 104006, Jan. 2025.
- [21] M. K. Ahmed *et al.*, "Based performance estimation of a slotted inverted F-shaped tri-band antenna for satellite/mm-wave 5G application," *Telkomnika*, vol. 22, no. 4, p. 773, Aug. 2024.
- [22] S. S. Rathore and S. Kumar, "A decision tree regression based approach for the number of software faults prediction," Sigsoft Softw. Eng. Notes, vol. 41, no. 1, pp. 1–6, Feb. 2016.
- [23] J. Piironen and A. Vehtari, "Comparison of bayesian predictive methods for model selection," *Stat. Comput.*, vol. 27, no. 3, pp. 711–735, May 2017.
- [24] F. Matloob *et al.*, "Software defect prediction using ensemble learning: A systematic literature review," *IEEE Access*, vol. 9, pp. 98754–98771, 2021.
- [25] R. Kumar, P. Kumar, and Y. Kumar, "Time series data prediction using IoT and machine learning technique," *Procedia Computer Science*, vol. 167, pp. 373–381, 2020.
- [26] E. Schulz, M. Speekenbrink, and A. Krause, "A tutorial on Gaussian process regression: Modelling, exploring, and exploiting functions," *Journal of Mathematical Psychology*, vol. 85, pp. 1–16, Aug. 2018.
- [27] S. M. Robeson and C. J. Willmott, "Decomposition of the Mean Absolute Error (MAE) into systematic and unsystematic components," *PLoS One*, vol. 18, no. 2, e0279774, Feb. 2023.
- [28] C. Willmott and K. Matsuura, "Advantages of the mean absolute error (MAE) over the root Mean Square Error (RMSE) in assessing average model performance," Clim. Res., vol. 30, pp. 79–82, 2005.
- [29] M. A. Haque *et al.*, "Machine learning-based technique for resonance and directivity prediction of UMTS LTE band quasi-Yagi antenna," *Heliyon*, vol. 9, no. 9, e19548, Sep. 2023.
- [30] M. A. Haque et al., "Broadband high gain performance MIMO antenna array for 5 G mm-wave applications-based gain prediction using machine learning approach," Alexandria Engineering Journal, vol. 104, pp. 665–679, Oct. 2024.
- [31] M. A. Haque et al., "Quasi-Yagi antenna design for LTE applications and prediction of gain and directivity using machine learning approaches," Alexandria Engineering Journal, vol. 80, pp. 383–396. Oct. 2023.
- [32] M. A. Haque et al., "Machine learning-based technique for gain and resonance prediction of mid band 5G Yagi antenna," Sci. Rep., vol. 13, no. 1, 12590, Aug. 2023.

Copyright © 2025 by the authors. This is an open access article distributed under the Creative Commons Attribution License which permits unrestricted use, distribution, and reproduction in any medium, provided the original work is properly cited ($\frac{\text{CC BY 4.0}}{\text{CC BY 4.0}}$).